IEEE Access
Multidisciplinary ⋮ Rapid Review ⋮ Open Access Journal

Received 6 June 2024, accepted 8 July 2024, date of publication 15 July 2024, date of current version 23 July 2024.

Digital Object Identifier 10.1109/ACCESS.2024.3427717

RESEARCH ARTICLE

Experimental Variable Band Hybrid Current Mode Control for High Power High Frequency Inverter in Electro Surgical Applications

MUHAMMAD MOHSIN RAFIQ[1], NASIM ULLAH[2], (Member, IEEE), LUKAS PROKOP[3], AND STANISLAV MISAK[3]

[1]Department of Electrical Engineering, CECOS University of IT and Emerging Sciences, Peshawar 25124, Pakistan
[2]Department of Electrical Engineering, College of Engineering, Taif University, Taif 11099, Saudi Arabia
[3]ENET Center, VSB-Technical University of Ostrava, 70800 Ostrava, Czech Republic

Corresponding author: Nasim Ullah (nasimullah@tu.edu.sa)

This research was funded by Taif University, Saudi Arabia, Project No. (TU-DSPP-2024-25).

ABSTRACT Electrosurgical generators (ESGs) are vital during medical operations, providing high-frequency electrical currents for cutting tissue and coagulation in surgery. Maintaining precise control over output power is challenging due to variable tissue loads. Inconsistent regulation can lead to undesirable surgical outcomes. This paper addresses this challenge through a novel Variable band hybrid current mode control (VBHCMC) technique. The study explores the limitations of existing approaches, such as peak current mode control (PCMC), emphasizing the need for improving control methodologies. The proposed VBHCMC method ensures stable output power, addressing issues associated with PCMC. It dynamically adapts the hysteresis band for variable load impedances, enhancing stability. The significance of this approach lies in its ability to combine the benefits of peak and valley current mode controls while maintaining a nearly constant switching frequency, significantly reducing steady-state errors. Results demonstrate significant reduction in steady-state errors compared to conventional PCMC. The proposed controller provides an effective solution to challenges faced in regulating output power during surgical procedures, enhancing safety and precision. The results have been verified in the MATLAB/Simulink environment, Processor-in-Loop (PIL) simulation in PSIM and using hardware validation.

INDEX TERMS Electrosurgical generators, current mode control, processor-in-loop, electrosurgical analyzer, hybrid current mode control.

I. INTRODUCTION

ESGs play a crucial role in medical procedures, generating high-frequency electrical currents to aid in tissue cutting and coagulation during surgical interventions [1]. ESGs typically operate across a frequency spectrum ranging from 300 kHz to 5 MHz's, and generate varying output power levels, hence catering to a range of surgical needs [2]. Typically, commercially manufactured ESGs operate at a frequency of approximately 500 kHz, with an allowable variation of ±100 kHz. Achieving precise control over the output power from ESGs poses a significant challenge due to substantial variations in tissue load characteristics encountered during surgical interventions [3].

Inconsistent regulation in controlling the output power of ESGs can potentially result in variations in surgical outcomes. Application of excessive power may cause undesired tissue injury, while insufficient power can lead to inconsistent tissue cutting [4], [5], [6]. The circuit's electrical impedance, which includes tissue and ESG, demonstrates significant variations

The associate editor coordinating the review of this manuscript and approving it for publication was Binit Lukose.

depending on the tissue. This variability spans from tens to thousands of ohms, as reported in previous studies [7]. To maintain consistent output power and mitigate the inherent heating impact, it is advantageous for the ESG to function as a continuous power provider. Nevertheless, it is imperative, from a pragmatic perspective, to restrict the sustained power output to predetermined levels of voltage and current (V-I) ensures the ESG's protection, by accompanying electrosurgical instruments with cables. Each component has limited capabilities for transporting electrical current and insulating voltage. Figure 1 illustrates I/V diagram showcasing the ideal output power characteristics of the ESG [8].

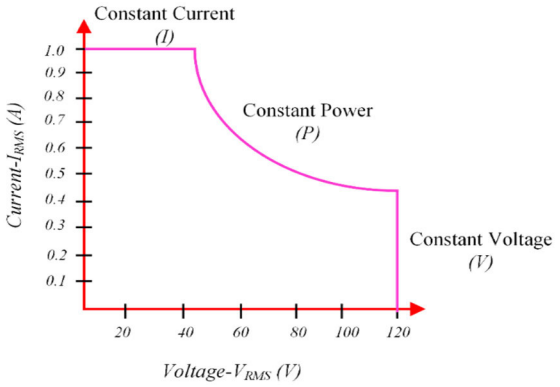

FIGURE 1. Desired output characteristic.

On the other hand, it is necessary to mitigate the risk of potentially dangerous electrical arcs during surgical procedures. Tissue segments with high impedance can generate increased voltages, causing sparking electrical discharges between the patient and electrosurgical tool. The curvature of these arcs results in a reduced contact surface area for the instrument, resulting in higher current density within the tissue. Consequently, this higher current density poses an increased risk of carbonization. Therefore, precise regulation of the ESG's maximum voltage output is essential to achieve the desired clinical outcomes. Ensuring a state of constant power in an alternating current output through proper control involves maintaining a stable average power level throughout each switching cycle [9], [10], [11].

The effective management of ESG operation involves two fundamental components: architectural design and control methodologies. In this context, ''architecture'' describes the actual circuit used to control output power of ESG. In this context, the term ''architecture'' pertains to the tangible circuitry utilized for the purpose of controlling and managing the power output of the ESG [12].

The author in [13] has proposed an approach for achieving swift control over output power, hence providing the benefit of generating a wide range of waveforms and current profiles. However, the methodology uses output waveforms in the form of square waves, which exhibit a substantially higher switching frequency. Consequently, this leads to an increase in switching losses. Square waves have the potential to generate super-harmonics that may pose a risk to tissues.

The introduction of the multi-resonant frequency (MRF) technique in [14], is to tackle the obstacles encountered by high-frequency inverters within the field of electrosurgery. However, it is important to note that MRF and other prevalent topologies are significantly dependent on resonant inverters [15]. The maximum output voltage and current of resonant inverters are inherently restricted due to their self-limiting nature [16]. Furthermore, these devices generate waveforms closely resembling sinusoidal patterns and exhibit limited adaptability in terms of output frequency, resulting in a significant disparity between peak instantaneous power and average power. Additionally, while soft switching inverters minimize switching losses, their efficiency is limited to a specific range of loads [3], [17].

In contrast, control techniques refer to the algorithms or strategies employed to control the power at output of an ESG. The researchers have proposed numerous low-frequency control techniques. These approaches encompass PI control [19], adaptive PID control, Neural Network Control (NNC) [18], with fuzzy control [20]. Recent advancements in sliding mode control (SMC) techniques, such as fixed time sliding mode control for DC/DC buck converters with mismatched uncertainties, have shown significant promise in addressing control challenges in variable load conditions [21]. Including these methodologies can provide a comprehensive overview of existing control techniques and their limitations.

Power measurements across several cycles are used by the control loops to get the required output power [22]. It is crucial to acknowledge that the efficacy of these strategies is limited in situations when the operating point of the converter experiences substantial variations. To effectively tackle the highlighted problems and enhance the output power, PCM is proposed in [23]. But PCMC has some limitations e.g., peak to average error (PAE), and artificial ramp induced error. The constraints mentioned in [30] have been addressed using expert knowledge based PCMC. But this solution is only proposed for fixed reference power, and when reference power changes this model does not adjust itself to desired output.

This paper introduces an innovative approach using a VBHCMC control to tackle these issues. Traditionally, the effective regulation of power output in the presence of varying load impedance conditions has posed challenges for the implementation of PCMC. To address this concern, our proposed control approach ensures sustained output at an elevated level throughout the valley point, subsequently resetting it to the peak point. This method aims to alleviate common errors associated with PCMC. Furthermore, the proposed approach allows operation at nearly constant switching frequency unlike hysteretic current mode control [24] in which switching frequency varies with varying load impedance.

Additionally, a novel methodology designed to mitigate errors by dynamically adapting the hysteresis band

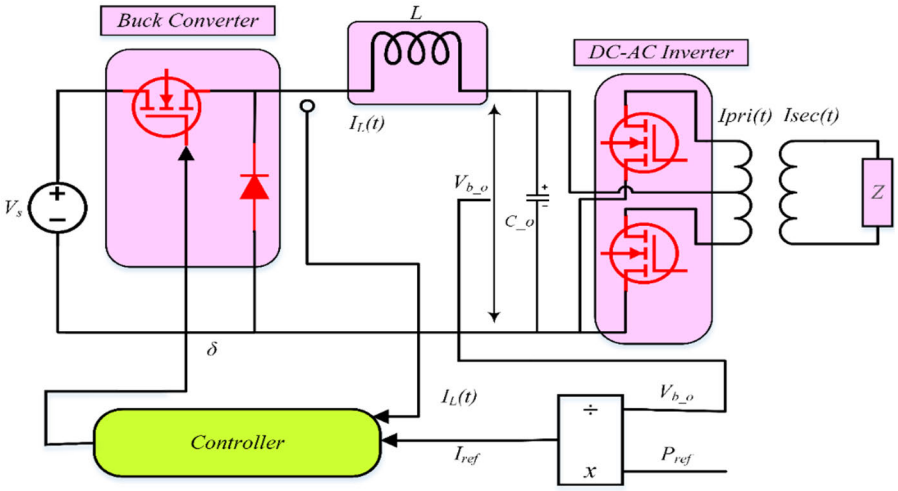

FIGURE 2. Circuit diagram of ESG.

in response to fluctuating load impedances, leveraging the band's dependence on the measured voltage. The adaptability inherent in this control approach are significant advantages, contributing to the improved stability and robustness of the controller. Consequently, this results in a more reliable and consistent regulation of power output. The key contribution of this studies is as follows:

The key contributions of this study are as follows:

- The development of an adaptive hysteresis band control mechanism that dynamically adjusts to fluctuating load impedances, improving the stability and robustness of the control system.
- The innovative integration of peak and valley current mode controls, maintaining a nearly constant switching frequency, which significantly reduces steady-state errors.
- Improved stability and precision in output power regulation, addressing the limitations of conventional PCMC.
- Extensive validation of the proposed VBHCMC method through MATLAB/Simulink simulations, PIL simulations in PSIM, and hardware implementation, demonstrating superior performance compared to traditional methods.
- Significant reduction in steady-state errors, ensuring more consistent and reliable operation of electrosurgical generators under varying load conditions.

II. SYSTEM DESCRIPTION

The ESG model comprises of a DC-AC inverter, a DC-DC buck converter, and proposed control, as illustrated in Figure 2. The system takes the input, denoted as V_s, which functions as a primary power source. The output voltage is produced using input, denoted as V_{b_o}. The input voltage is first adjusted to a lower level by the DC-DC buck conversion and transformed into high frequency AC power by DC-AC inverter. The direct current (DC) voltage must be converted into a high-frequency alternating current (AC) voltage via a DC-AC inverter, which will subsequently be utilized to electric power the ESG.

The variable $I_L(t)$ denotes the current passing through the inductor, while V_{b_o} refers to the output voltage of the input voltage of the high-frequency inverter and the buck converter. The variable $I_{pri}(t)$ denotes prime current of the isolated transformer, whereas $I_{sec}(t)$ refers to the secondary current of the transformer which is supplied to the surgical tool that the physician is using. The tissue impedance denoted by the symbol Z. The impedance is represented by a resistor to mimic and assess the efficacy of the ESG.

A. DC-DC BUCK CONVERTER

The initial setup of the ESG system involves the integration of a buck converter. The buck conversion is a crucial element of the ESG, utilized to decrease an elevated input voltage to a diminished output level. By utilizing pulse-width modulation (PWM), the voltage is effectively regulated by manipulating the duty cycle of a switching component, commonly a transistor as depicted in Figure 3.

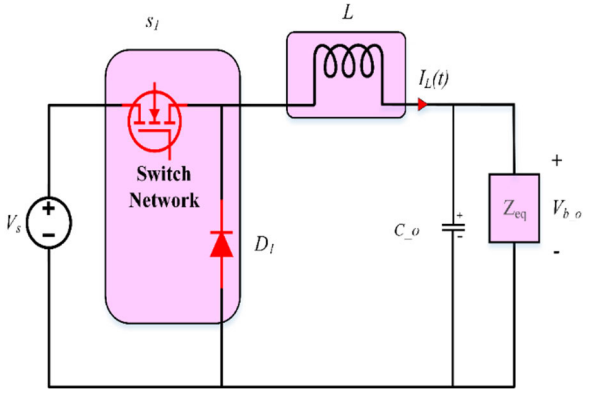

FIGURE 3. Buck converter circuit.

The fundamental circuit involves several components, including an input voltage V_s, an inductor (L), an output capacitor (C_o), and a load (Z_{eq}). The operation of this system entails the periodic storage of energy in the inductor during the switch-on phase, followed by its subsequent release to the output during the switch-off phase.

The buck converter's mathematical representation consists of state-space s (1)-(2), which contain its dynamic properties by expressing key variables. Table 1 presents the buck converter parameters. (1)-(2) describe the behavior of output voltage (V_{b_o}), inductor current (I_L) accounting for output capacitor voltage C_o, duty cycle, and input voltage.

$$\frac{dI_L}{dt} = (V_s - V_{b\_o})/L \tag{1}$$

$$\frac{dV_c}{dt} = (I_L - I_{out})/C\_o \tag{2}$$

TABLE 1. Buck Converter parameters.

Parameter	Value	Unit
Input Voltage V_s	48	V
Maximum_output_voltage (V_{b_o})	45	V
Maximum_average_current (I_{avg})	3	A
Dutycycle (D)	-	variable
Switching_frequency (f_s)	1	MHz
Inductance (L)	100	uH

B. DC-AC HIGH FREQUENCY INVERTER

Figure 2 depicts the ESG model, which consists of a buck converter coupled with a push-pull inverter connected in series. While, Figure 4 shows a high-frequency converter, specifically a DC-AC push-pull inverter. This type of inverter is used to convert DC power into AC power. It operates using two switches (transistors) that alternate between being turned on and off to produce AC output. As one switch conducts, the alternate stays off, creating a "push-pull" motion that moves current from the transformer to the load. Transformer center tap connected to the DC input. The DC input is linked to the transformer's center tap. When a transistor is active, current flows through one half of the primary winding, meanwhile, the transistor conducts across the other half. This split primary winding generates an AC output in the secondary winding.

The fluctuation between the turn on/off states of the transistors causes the transformer to generate an AC output. Detailed specifications for the inverter circuit are explained in Table 2.

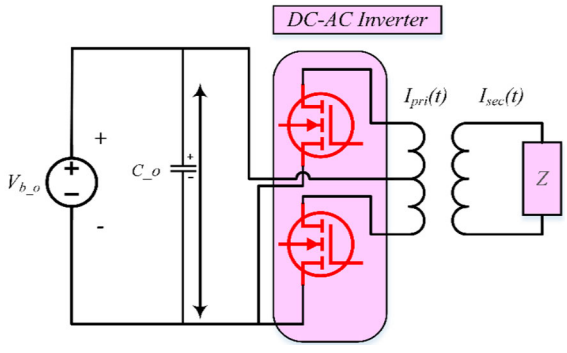

FIGURE 4. High frequency push pull DC-AC inverter.

TABLE 2. Inverter specification.

Specification	Value	Unit
Max_Input_DC_voltage (V_{b_o})	45	V
Max_output_voltage (V_{RMS})	120	V
Maxoutput current (I_{RMS})	1	A
Switching_frequency (f_S)	500	KHz
Turns ratio of a transformer	1:3	-
Impedance limit	10-340	Ω
Reference power Range	50	W

III. MODES OF OPERATION OF ESG

A. CONSTANT CURRENT MODE

The generator's design ensures that it can steady the output current in a constant-current mode, independent of the load's impedance. The constant DC current source property of the buck converter output under (CMC) documented extensively in [25]. Figure 2 illustrates an instance of a PMC buck converter controller that is interconnected in a sequential configuration with a DC-AC inverter. An alternating current (AC) source with the same magnitude as shown in Figure 5 is the output that results from the inverter DC to AC working on a 50% duty cycle. Therefore, desired alternating current constant current source is attained.

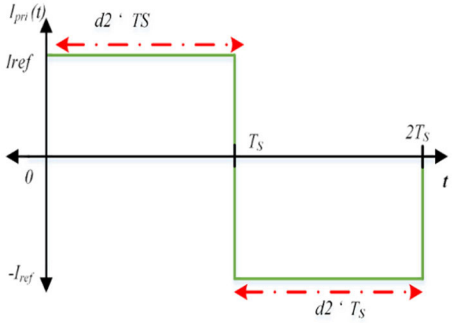

FIGURE 5. Buck converter CMC output current control.

Averaged switch modeling can be used to achieve the result of a PCMC control buck converter, which allows for the characterization of the converter as a continuous current supply. (3) and (4) present the average current and average voltage, respectively.

$$\langle I_1(t)\rangle_{T_s} = d\,(t)\,.\langle I_2(t)\rangle_{T_s} \tag{3}$$

$$\langle v_2(t)\rangle_{T_s} = d\,(t)\,.\langle v_1(t)\rangle_{T_s} \tag{4}$$

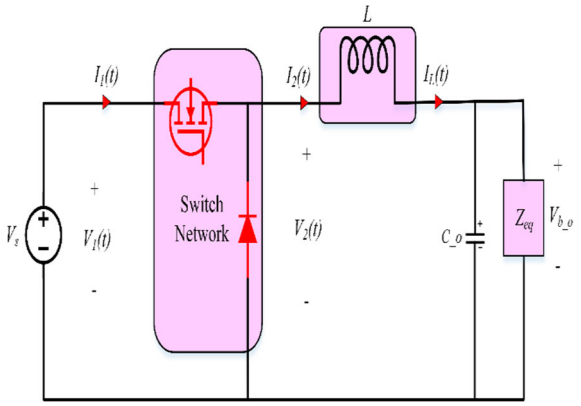

FIGURE 6. Buck converter switch configuration.

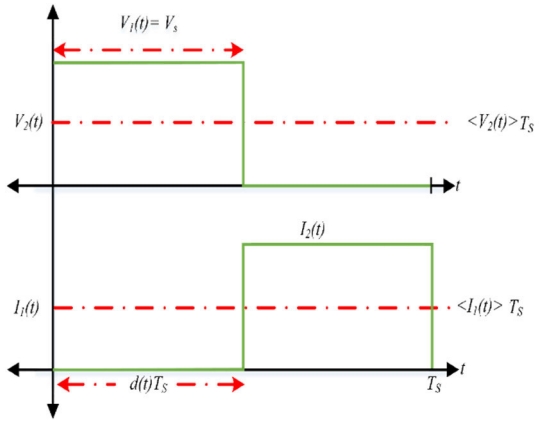

FIGURE 7. Voltage and current waveform behavior of buck converter.

PCMC effectively regulates mean inductor current inside the prescribed limit of the control current, as shown in following:

$$\langle I_2(t)\rangle_{T_s} = \langle I_L(t)\rangle_{T_s} = \langle I_{ref}(t)\rangle_{T_s} \tag{5}$$

B. CONSTANT POWER MODE

The generator has been specially developed to regularly generate a steady output power in the constant power mode, regardless of any variations in the load impedance. (6) represents the power source to the inverter switch circuitry with help of DC-DC buck converter in the constant power mode.

$$P = I_L\,(t)\,.\delta.V_s \tag{6}$$

If the maximum current through an inductor is I_{ref} in PCMC, then (6) changes to:

$$P = I_{ref}\,.\delta.V_s \tag{7}$$

The DC-AC inverter converts voltage on a 50% duty cycle while maintaining magnitude regarding the DC-DC buck voltage. Consequently, the current denoted as $I_{pri}(t)$ is equivalent to both I_L(t) and I_{ref}. (7) encompasses two time-varying variables, namely I_{ref} and δ, for which it is possible to calculate the output power P under certain load conditions.

To get the value of I_{ref}, rearrange (7) then.

$$I_{ref} = \frac{P}{\delta \cdot V_g} \tag{8}$$

Average inductor current I_{ref} (t) is described by (8).

C. CONSTANT VOLTAGE MODE

In order to maintain a consistent output voltage, the duty cycle should be maintained at a low level of the peak current mode (PCM) controller, as shown in Figure 8.

To provide a steady output voltage, it is necessary to limit the duty cycle for the peak current mode (PCM) controller, as depicted in Figure 8.

Also, it is essential to recognize how employing duty cycle restriction as an option to provide a consistent voltage output using a PCM controller can have certain disadvantages, such as diminished effectiveness and increased output voltage ripples. Imposing limitations on the duty cycle used by the PCM controller within a (DC-DC) converter results in the converter functioning without feedback, potentially causing disruptions.

This section provides an overview of the electrical schematic of an ESG, which includes DC-AC inverters and DC-DC buck conversion. Furthermore, we presented a detailed representation of the optimum output waveform for an ESG in results. This included the three main approaches to operation: constant electrical current, constant power, and continuous voltage.

IV. LIMITATION OF PCMC

The PCMC method is frequently employed for regulating the peak current in the inductor of power converters. Nevertheless, it is essential to acknowledge that within actual power sources, three primary forms of defects may arise: artificial ramp error, transient error, and PAE.

A. PEAK TO AVERAGE ERROR (PAE)

Peak-to-Average Ratio shows how much the inductor current fluctuates between its average and maximum values when there's significant ripple current [26]. Unique compensatory approaches could be utilized in reducing or eliminating the PAE in specific peaks current mode (PCM) control [25]. Nevertheless, it is important to note that these strategies may not yield desirable results in situations when there is significant variation in the operating point of the converter. The technique used to determine a current control threshold aims to minimize fluctuations in inductor current and establish a stable inductor current level required for maintaining a consistent power output across various load impedances. However, this approach becomes unreliable when a substantial quantity of inductor current ripple is encountered [20]. The discrepancy between the average inductor current and the control current limit can cause a considerable steady-state error in the output power, as mentioned in [27].

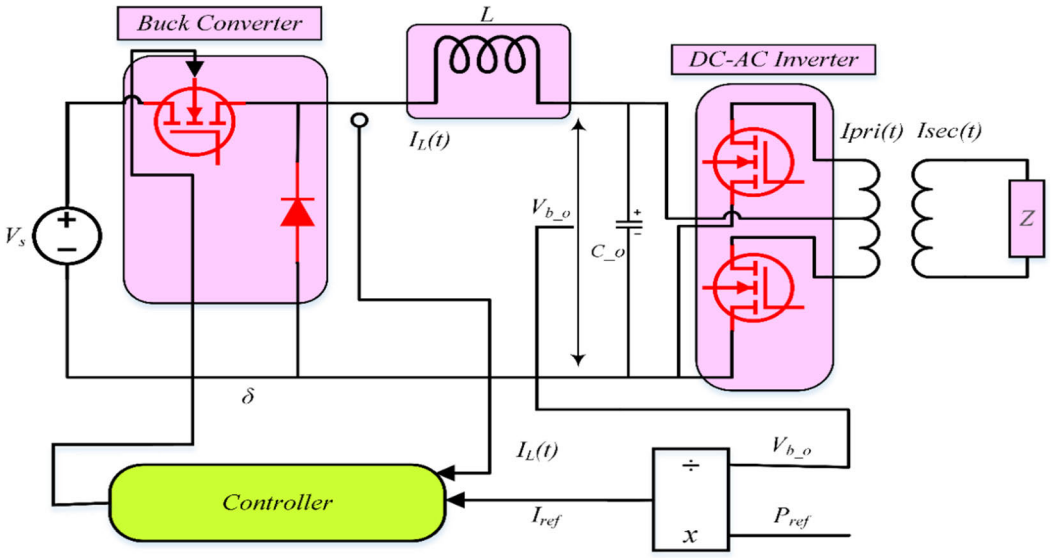

FIGURE 8. Max voltage limitation used duty cycle.

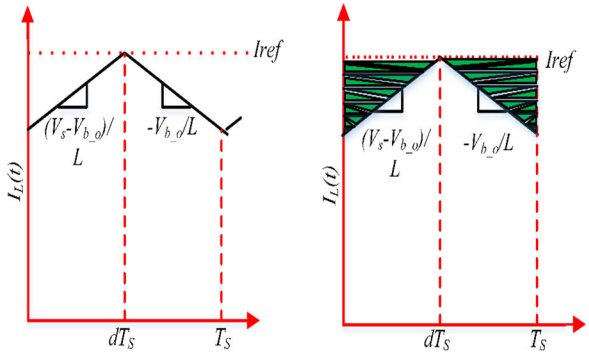

FIGURE 9. Steady-state inductor current [28].

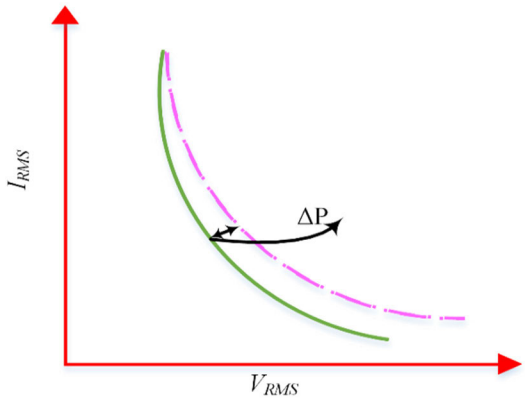

FIGURE 10. PAE in ideal curve using PCMC [28].

Significant inductor current ripple causes the $\Delta I_L.(T_s) = I_{ref}$ to be inappropriate. In this scenario, $\Delta I_L.(T_s) = I_{ref}$ holds true, as demonstrated in the data presented in Figure 9, which demonstrates that the maximum and mean inductor current value may not converge.

Figure 10 illustrates the influence of fluctuations on the highest and averaged outputs of a buck converter.

B. ARTIFICIAL RAMP ERROR (ARE)

The PAE within PCM controller can be impacted by introducing an artificial ramp, particularly for converters with duty cycle equal to or exceeding 50%. This compensatory ramp enhances noise rejection in measured inductor current and stability. Figure 11 illustrates how duty cycle variations affect *Iref* (t) due to the compensatory ramp. It is crucial to assess if variations in *Iref* (t) average values are influenced by the compensatory ramp's size. Figure 12 highlights the consequential impact on a dependable power source, revealing noticeable errors with low output impedance and an increasing error magnitude with higher output impedance values. This exploration underscores the significance of compensatory ramp considerations in mitigating errors for reliable power sources.

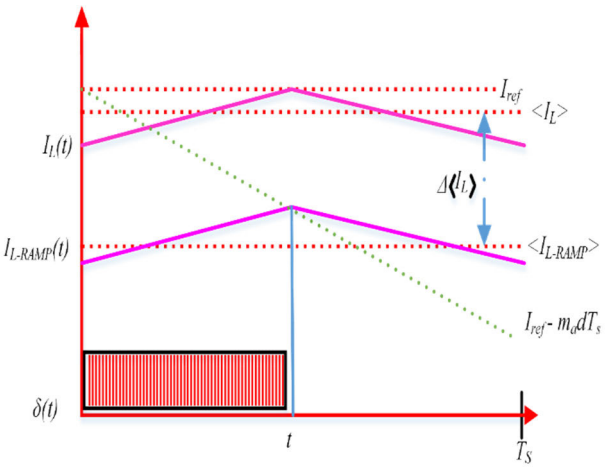

FIGURE 11. PCM control with/without ARE [28].

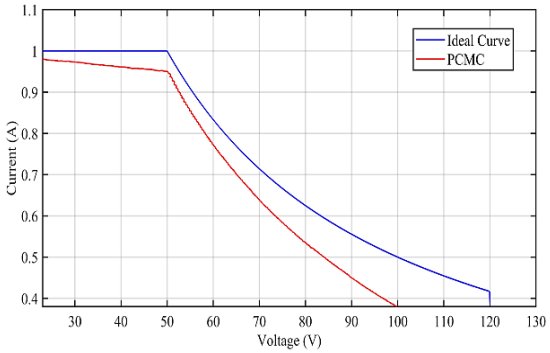

FIGURE 12. Impact of PAE and ARE [28].

C. TRANSIENT ERROR

Figure 13 depicts the load stepping event occurring during a time interval of 0.2 milliseconds, demonstrating a power spike becomes increasingly prominent by the rise of L values. To enhance the operational efficiency in the PCM buck converter under abrupt fluctuations, ensuring the complete transfer of all the conserved energy within the inductor to the circuit's load is crucial. Thus, lowering the inductor's value can be a realistic technique for improving the converter's performance.

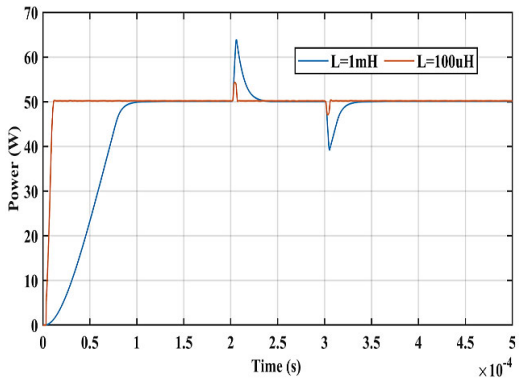

FIGURE 13. Transient response during step load [28].

In summary, the presence of non-idealities has the potential to impose limitations on PCMC efficiency in power converters. Nevertheless, it is possible to address these constraints and enhance the converter's performance by implementing diverse compensation mechanisms and optimization approaches.

V. PROPOSED CONTROLLERS

The existing approaches for Current mode control generally consist of Average current mode control (ACMC), PCMC, and Valley current mode control (VCMC) [20], [21], [22]. Figure 14 represents PCMC, whereas Figure 15 portrays a block schematic illustrating VCMC.

PCMC includes the regular activation of the transistor while clock pulses serve as the authorized signal for setting the operation. Furthermore, when the inductor current meets

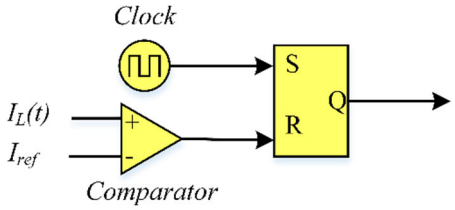

FIGURE 14. Peak current mode controller (PCMC).

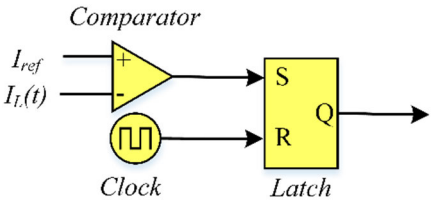

FIGURE 15. Valley current mode controller (VCM+C).

the peak current control signal, a reset command occurs, causing the transistor to deactivate.

Nonetheless, it is vital to realize that subharmonic oscillation might develop in PCMC when the duty cycle exceeds 0.5 [28].

The PCMC current waveform is depicted in Figure 16, which corresponds to the operational procedure described in Figure 14. As illustrated in the diagram, as duty cycle surpasses 0.5, the amplitude of the current disturbance increases, hence the occurrence of sub-harmonic oscillation.

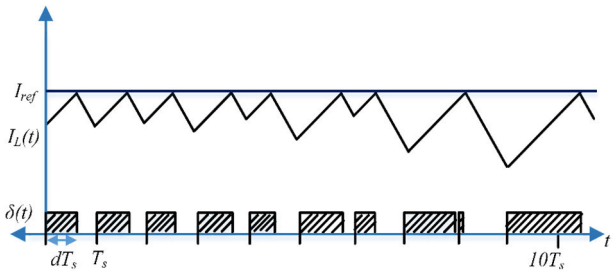

FIGURE 16. PCMC waveforms illustrating instability [29].

VCMC, as opposed to PCMC, entails the periodic deactivation of the transistor during specific time intervals inside the clock pulse, which will be denoted as the reset signal. Likewise, when the current flowing through the inductor becomes synchronized command signal with the minimum current, a predetermined signal is produced, resulting in the activation of the transistor. Nevertheless, it is crucial to acknowledge that CMC might experience sub-harmonic oscillation under specific conditions, specifically when the duty cycle falls below 0.5 [24].

A. PROPOSED VARIABLE BAND HYBRID CURRENT MODE CONTROL

That work presented in unique VBHCM controller that incorporates peak and valley currents into its design. The controller

we have proposed exhibits resemblances to the hysteretic current-mode controller. In comparison to conventional hysteresis current-mode control techniques that often utilize a predetermined hysteric band [25], [26], [27], our controller exhibits the capability to adaptively modify the current band gap in a flexible and responsive manner. The objective of this modification is to reduce the extent of fluctuations in switching frequency, even in the presence of variable impedance.

It is critical to maintain a steady frequency despite differences in impedance and desirable power levels. To attain this objective, it is imperative to comprehend the correlation between the intended power for a constant impedance and the current band gap. Furthermore, a comprehensive understanding of the band gap pertaining to the entire range of impedance that corresponds to a constant power is necessary. The steady-state inductor current waveform is depicted in Figure 17.

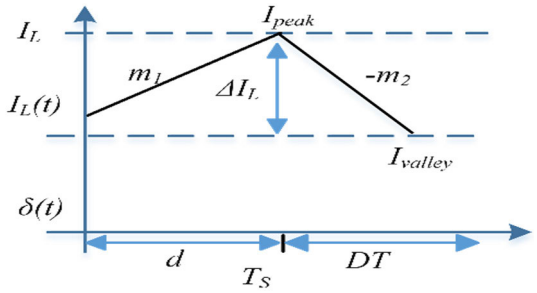

FIGURE 17. Steady state inductor current.

In this scenario, m_1 symbolizes how fast the inductor current rises, and DT indicates the moment when this rise happens. The band gap, ΔI_L, changes based on impedance and output voltage variations to keep the power output consistent.

(9) defines the current band gap, ΔI_L, where f is the PWM frequency, and V_{b_0} is the buck converter output voltage, Vs buck converter input voltage and L is the inductor value.

The current band gap is defined by (9), where L is inductor value, f is the PWM frequency, Vs is input voltage to buck converter.

$$\Delta I_L = \frac{V_{b\_0}.(V_s - V_{b\_0})}{V_s \cdot L \cdot F} \tag{9}$$

$$I_{peak\_ref} = I_{ref} + \frac{\Delta I_L}{2} \tag{10}$$

$$I_{valley\_ref} = I_{ref} - \frac{\Delta I_L}{2} \tag{11}$$

The determination of the maximum current command is performed according to (10), whereas the calculation of the minimum current command according to (11). In this case, the variable I_ref refers to the current command signal generated by multiplying the desired power at output voltage. Figure 18 shows a suggested block architecture for the VBHCMC, which graphically reflects the control system.

Upon comparing the strategy described in Figure 18 with a previous approach illustrated in Figure 14 [19], a notable

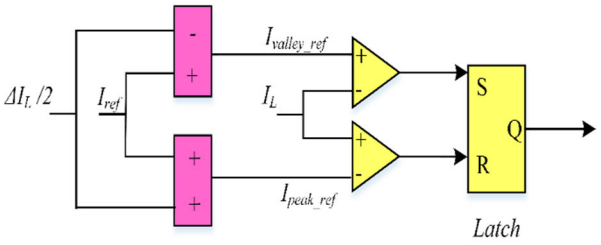

FIGURE 18. Proposed VBHCMC.

disparity becomes apparent. In the previous approach, slopes are utilized to mitigate the occurrence of sub-harmonic oscillation. However, the task of modifying the slope to accommodate impedance variations is a significant challenge. The controller under consideration effectively tackles this difficulty by employing software to determine the bandgap, hence providing the benefit of automatic adjustment to a constant frequency in the presence of varying resistance. Additionally, the suggested controller successfully addresses inherent faults associated with PCM regulation, including PAE and compensation slope error.

Figure 19 shows two waveforms: one created using VBHCMC and a theoretical current-voltage (I-V) curve. The ideal curve corresponds to the waveform shown in Figure 1, which displays a typical curve demonstrating the identical features of RMS voltage of 120V, and an RMS current of 1A and steady power of 50 W.

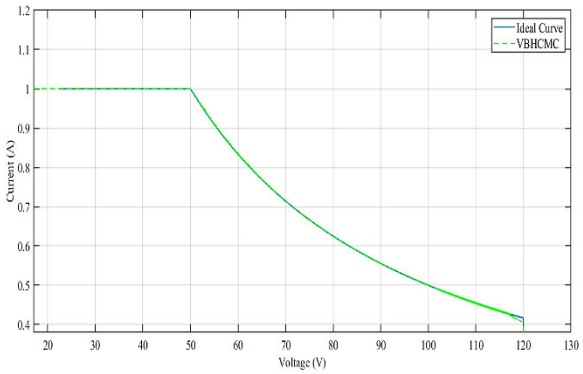

FIGURE 19. Current comparison between proposed VBHCMC and ideal curve.

VI. SIMULATION, PIL VALIDATION AND HARDWARE IMPLEMENTATION

A. SIMULATION RESULTS

The demonstration of the incorporated VBHCMC in this section aims to rectify errors in power limitations associated with PCMC. In order to accomplish our goal, we performed simulation studies utilizing the mathematical representation of the ESG and the tissue load. A power source has been imitated using a single-phase converter coupled with buck converter. It engaged with the tissue load, which appears as resistance. Numerous simulations are run to compare the efficiency of PCMC control with the proposed VBHCMC. The simulations are categorized into two distinct categories,

one utilizing VBHCMC control and the second employing standard PCM control.

The simulations aimed to demonstrate the improved efficacy resulting from the proposed VBHCMC approach. Emphasizing the main objective for such simulations is to demonstrate the effectiveness of VBHCMC control, distinguishing it from conventional PCM control methodologies.

Figure 20 depicts the V-I ESG trajectory spanning a broad spectrum of load changes. It displays the system's efficiency with the proposed Variable Band Hybrid Control Method (VBHCMC) and PCMC. The load ranged linearly from (0-340 Ω). The simulations included selecting certain load values within the range, monitoring output power at intervals, and modifying load resistance in the Simulink model to analyze the influence of VBHCMC control on output power. Next, the identical technique was duplicated across a range of load values that cover the recommended impedance spectrum, ultimately achieving an optimal load of 340 Ω. Such an iterative method allowed for a thorough analysis of the system's reaction for various load circumstances within simulation setting. Similarly, process duplicated for power generation using conventional PCMC in the Simulink environment, acting like a standard comparison with VBHCMC control. The collection of power data for each load value allowed for the creation of a graph that demonstrates within the simulated environment, the connection between demand fluctuation and power produced.

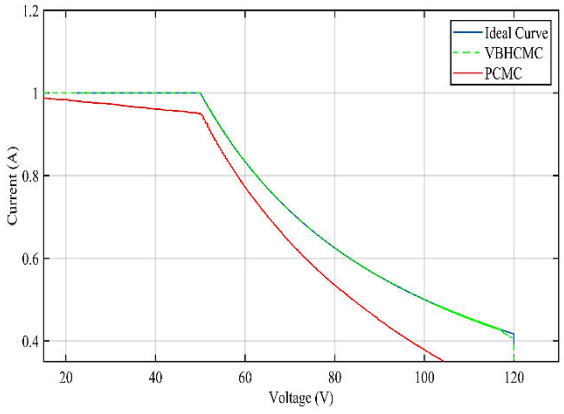

FIGURE 20. Comparison of voltage and current waveforms between Ideal, EK-PCMC.

The VI curve represented in Figure 20 summarizes data collected to determine load values that cover every aspect of impedance. Every dot on the curve signifies every particular load value and the same output power collected throughout Simulink, providing a comprehensive representation of the system's performance.

The vital finding from the VI curve analyzed how the VBHCMC controlled during the Simulink simulate effectively sustains the desired power reference over the whole range of loads. In contrast, the conventional PCMC control Simulated in Simulink shows artificially induced ramp errors

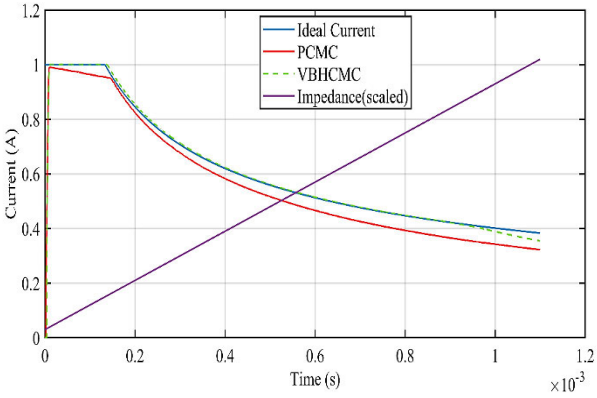

FIGURE 21. Output current contrast against load variations.

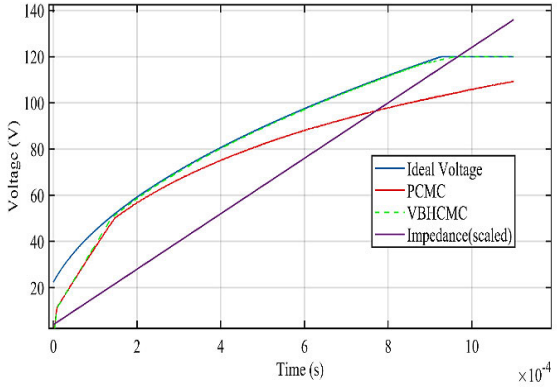

FIGURE 22. Output voltage contrast against load variations.

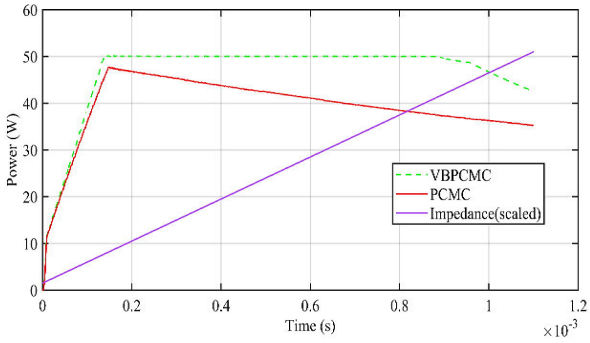

FIGURE 23. Output power curve with reference to time.

and steady-state errors created errors when the load changes. This emphasizes the advantages of VBHCMC control.

Figure 21 portrays the Root Mean Square (RMS) current of the ESG, utilizing corresponding simulations as in Figure 20. While Figure 20 displays the V-I curve obtained through V-I measurements, Figure 21 scrutinizes the current over time. This depiction allows a detailed examination of current fluctuations under VBHCMC and conventional PCMC control, providing insights regarding dynamic behavior of the whole system by responding to load variations.

The downscaling of the impedance curve is done using a factor of 0.003 to improve comparability. By dividing the peak current curve value by the peak impedance value, this

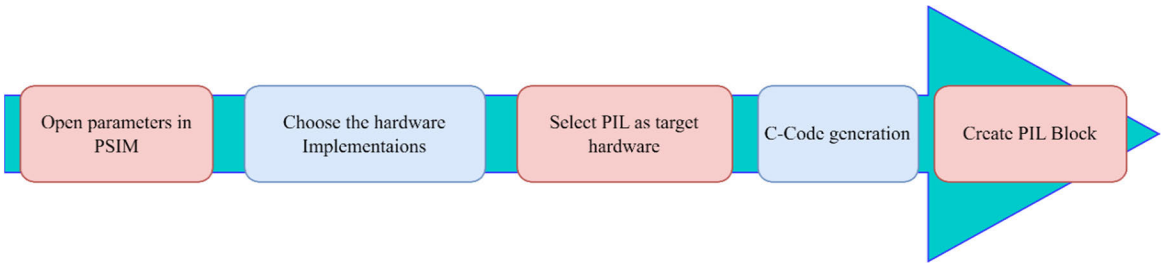

FIGURE 24. PIL simulation steps.

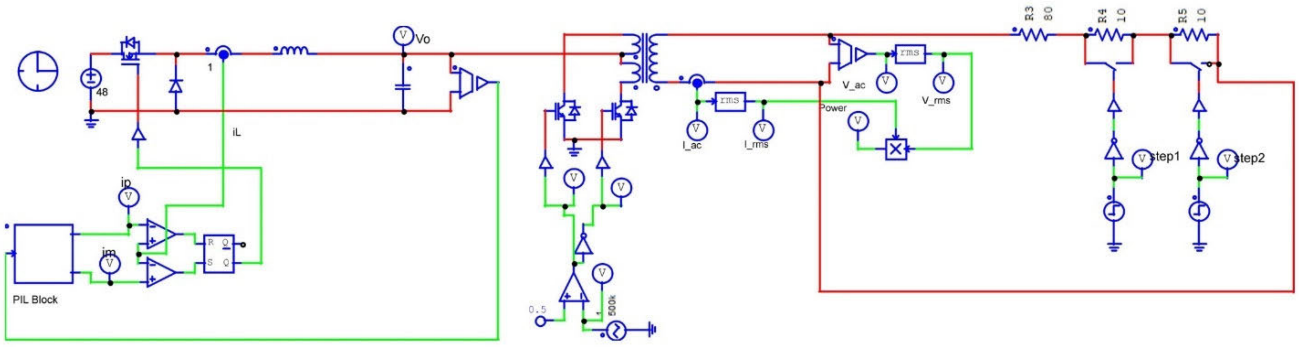

FIGURE 25. PIL implementation.

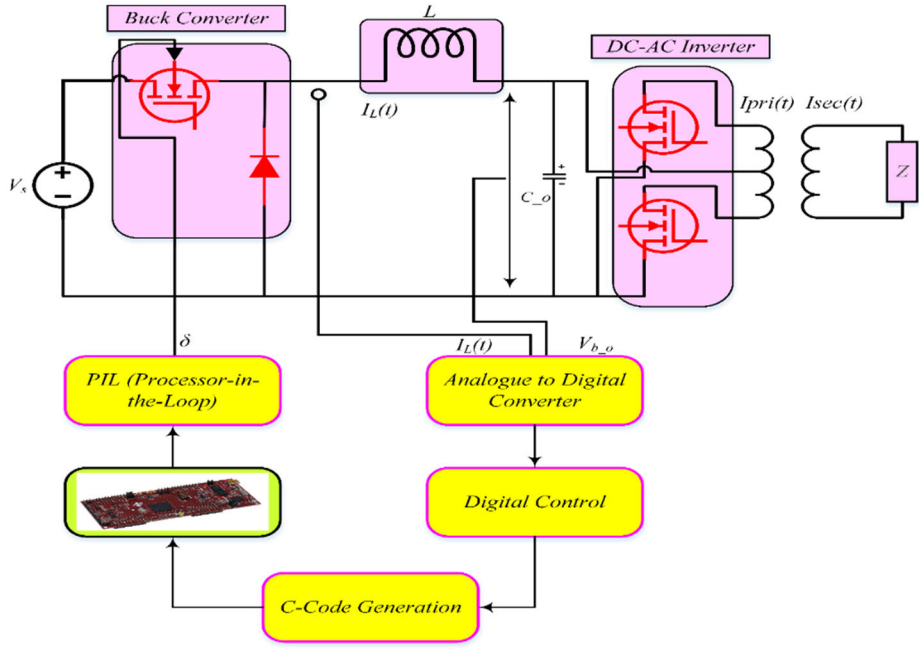

FIGURE 26. PSIM implementation of converter with PIL block.

scaling is calculated, enabling a more pronounced representation of current characteristics. This adjustment optimizes the clarity and precision of the comparison with the existing curve.

Figure 20 presents a comprehensive representation of load fluctuations in terms of a V-I curve, illustrating the behavior of systems. In contrast, Figure 21 allows for a more comprehensive evaluation of the current's temporal behavior. This investigation provides valuable information into the changing electrical current of the ESG unit under various load scenarios.

Upon scrutinizing both sets of data, it is evident that the Root Mean Square (RMS) current achieved through VBHCMC control continuously surpasses that acquired with conventional PCMC control across all levels of load fluctuations. It further strengthens the evidence that supports the

efficacy of EK-PCMC control for sustaining consistent robust electrical output under multiple load circumstances.

Figure 22 exhibits the ESG device Root Mean Square voltage (V_{RMS}) across diverse load fluctuations. In accordance with Figure 21, simulations are performed using the methods described in Figure 20, with a particular emphasis on clarifying the voltage characteristics.

In order to enhance compatibility alongside the voltage curve, the impedance curve is reduced by a value of 0.4. The factor used for scaling is calculated by dividing the highest voltage by the maximum impedance.

The data demonstrates if the RMS voltage (V_{RMS}) attained using EK-PCMC control regularly exceeds that reached with the conventional PCMC controller, regardless of the degree of load variability. This discovery highlights the efficiency of EK-PCMC control in constantly sustaining a maximum and much steady voltage output despite various changes in load.

Figure 23 depicts the power output of the ESG device across diverse situations of load fluctuations. In keeping with the methodology described in Figure 21 and 22, the simulations followed the same strategy as detailed in Figure 22, with a specific emphasis on power characteristics. The impedance curve is scaled down by 0.1 factor in order to make comparisons with the power curve easier.

Figure 23 shows a comparison of reference power to power achieved using VBHCMC and PCMC. The following impedance curve shows the influence of different impedance stages, increasing gradually from (10-340 Ω) throughout the measurement.

The ESG early on runs in constant current mode, then at 0.17 ms it changes to constant power mode as impedance grows, and finally at 0.97 ms it transforms to constant voltage mode as the impedance exceeds 200 Ω.

TABLE 3. Results Comparison between Proposed VBHCMC and PCMC.

Controller	Integral Square Error	Integral Absolute Error
PCMC	0.3199	0.0175
VBHCMC	0.0824	0.0036

Table 3 clearly indicates a fourfold superiority of VBHCMC over conventional PCMC in mitigating power error. Employing VBHCMC controllers can significantly enhance the performance of ESG's, particularly in terms of precise power regulation, as evidenced by the comparative results.

VII. PIL VALIDATION

The PIL has become more valuable for implementing power electronics applications due to its ability to produce accurate and realistic results. Executing some tests in a converter-inverter operation can be challenging in practical settings due to the requirement for variations in switching states circumstances. However, implementing this is straightforward using a PIL approach based on the TMS320F28379D

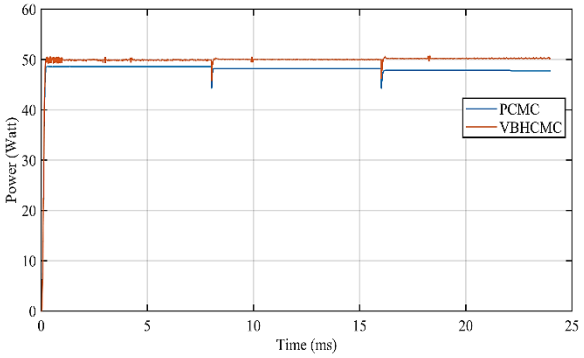

FIGURE 27. Power comparison using PIL simulations between VBHCMC and PCMC.

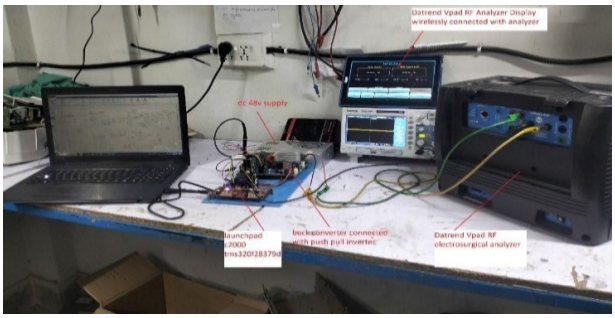

FIGURE 28. Hardware Testbench Setup of the proposed VBHCMC.

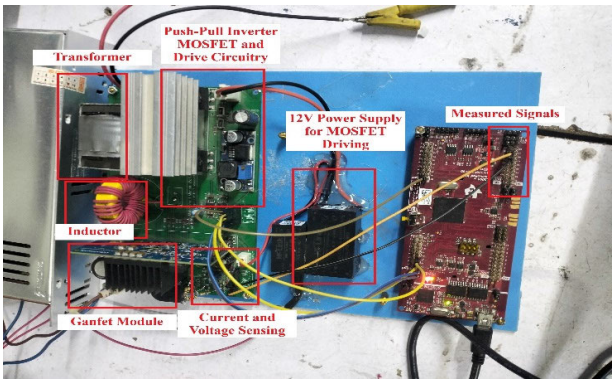

FIGURE 29. Hardware prototype of the proposed VBHCMC.

DSP chip. This study validates the effectiveness and achievability of the VBHCMC method by employing a processor in the loop simulations. Figure 24 represents the technique for setting up the PIL experiment on the PSIM platform employing the DSP chip TMS320F28379D, while Figure 25 depicts the block diagram of implementing PIL.

PSIM software creates C-code for the proposed control method. This C-code is then compiled using the Code Composer Studio, resulting in the generation of a .out file. The PIL PSIM block then uses the compiled file to enable PIL simulation. The .out file replicates the control algorithm's activities throughout the PSIM PIL simulation.

After successfully completing the PIL simulation, the built .out file is loaded onto the TMS320F28379D DSP chip. The real-time control method is then implemented using the DSP board, confirming its efficacy in an embedded system setting.

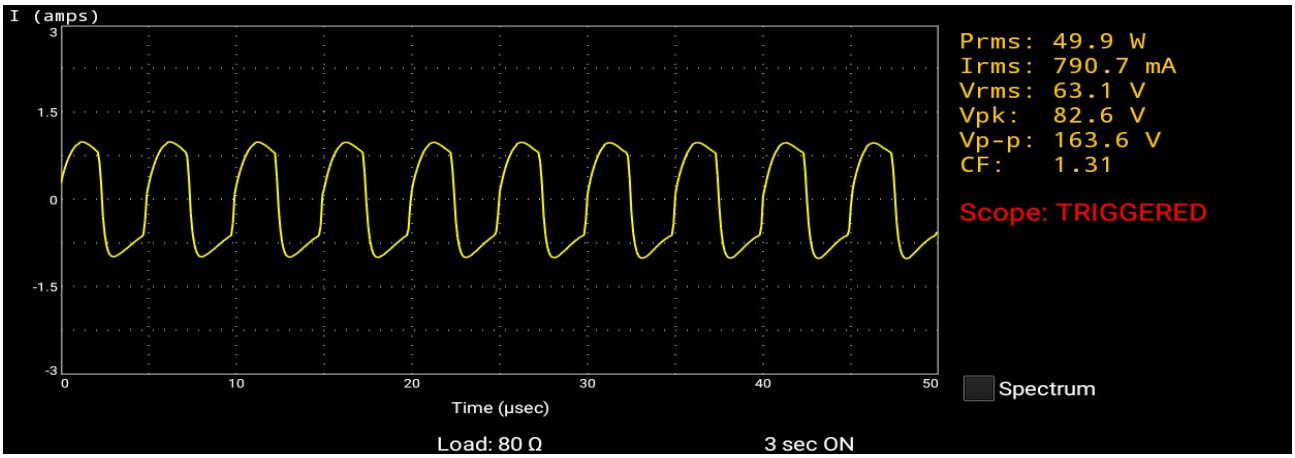

FIGURE 30. Datrend VPAD RF measurement at 80 Ohms.

Figure 26 illustrates the use of a comparative testing approach with PSIM software to show the effectiveness of the recommended controller. A real-time PIL test is used to generate simulation results in order to evaluate the control scheme's efficacy.

Load step transitions take place at t = 8 ms and 16 ms for 90- Ω and 100 Ω loads respectively. The initial load impedance is 80-ohm. The same tests in the PIL simulations are assessed for both the proposed and PCMC.

Figure 27 shows the obtained results, highlighting the significant reactions to changes in load steps using the VBHCMC and PCMC methods.

Moreover, the results clearly demonstrate VBHCMC's superior control capabilities over PCMC, especially when dealing with changes in load impedance. It is evident from a comparison of the two strategies that the proposed control strategy performs better at controlling power.

VIII. EXPERIMENTAL HARDWARE IMPLEMENTATION

The VBHCMC system was implemented using an advanced hardware configuration.

This configuration involved connecting a prototype buck converter series with a push-pull inverter in a seamless manner. The primary component of the system, the buck converter, efficiently controlled the input voltage and ensured accurate control to reach the required power levels. The push-pull inverter, which plays a crucial role in forming the output waveform and ensuring its exceptional quality, is successfully connected to the main electrical conditioning component. A C2000-Launchpad with F28379D series chip, a microcontroller-based architecture with a wealth of advanced features and processing power, is used to synchronize the control mechanism. The Launchpad allowed for immediate control and monitoring of the buck converter, allowing for the smooth application of the VBHCMC method. Figure 28 and 29 illustrate the hardware prototype which employs a DC 48V power supply for the buck converter input, a DC 5V supply to operate the ganfet module, a DC 12V supply to operate the MOSFET and testing circuits. Moreover, the experimental setting was significantly influenced by the inclusion of a Datrend VPAD RF analyzer, which featured an integrated load and measurements.

The system's performance was thoroughly assessed using the Datrend VPAD RF analyzer, which includes an integrated oscilloscope and offers measurements for RMS voltage, RMS current, power, and crest factor. The oscilloscope feature of the Datrend VPAD RF analyzer enabled detailed examination of waveforms, while the RMS voltage and current measurements offered an understanding of the RMS values. Additionally, the analyzer made power and crest factor measurements easier, enabling comprehensive evaluations of the VBHCMC system's effectiveness and waveform quality.

The experimental results obtained from the Datrend VPAD RF analyzer, using a 50 W reference power, offer a comprehensive analysis that confirms the efficacy and dependability of the VBHCMC approach in the field of ESG. The precise measurements taken under different load levels offer a detailed comprehension of the system's behavior and its ability to respond to changing load scenarios.

Figure 30 exhibited a remarkable output power of 49.9 watts, showcasing the VBHCMC's capacity to maintain accurate control around the reference power level. The RMS voltage, which is an essential measure of the effective voltage of the system, is measured at 63.1 volts, demonstrating the method's capacity to reliably control the voltage output. The RMS current, for evaluating the average current flow, was measured at 790.7 milliamperes. This indicates that the VBHCMC is very skilled at delivering consistent current even when faced with different load impedances. The Crest Factor was determined to be 1.31. The measurements at 100 ohms resulted in the following values: Figure 31 demonstrated an output power of 49.8 watts, highlighting the VBHCMC's ability to maintain consistent power levels under various load conditions. The RMS value, recorded at 70.5 volts, indicates that the VBHCMC method successfully controlled the voltage output, even when the load resistance was raised. The RMS current, quantified at 706.4 milliamperes, demonstrates the technique's flexibility in handling varying load

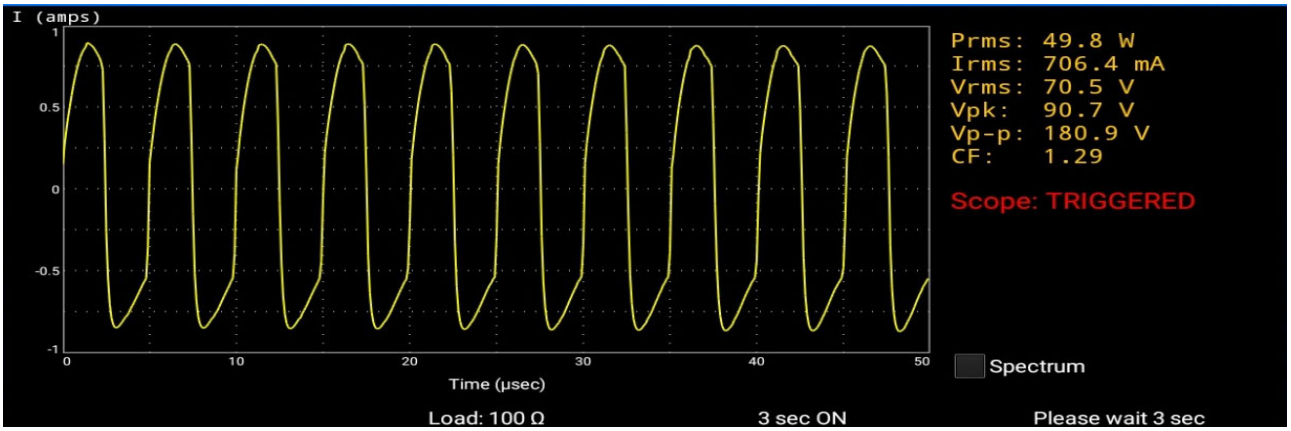

FIGURE 31. Datrend VPAD RF measurement at 100 Ohms.

situations, guaranteeing a regulated and consistent flow of current. The system's ability to maintain a waveform of superior quality free of distortion is validated by the 1.29 Crest Factor. The outcomes show how well the VBHCMC approach works to provide exact stability and control under dynamic load situations. The system's potential to greatly improve the performance of ESG in crucial medical applications is shown by its ability to reliably sustain reference power levels despite changing impedances. Because of its ability to adapt to changing load conditions, the VBHCMC approach is a desirable solution for reducing the difficulties related to power control in surgical procedures. This ultimately results in improved electrosurgery safety, precision, and general efficacy.

IX. CONCLUSION

This study introduces a novel VBHCMC method for electrosurgical applications, addressing the limitations of traditional PCMC. PCMC with slope compensation are common for swift response, but high slope values during voltage changes can introduce errors. Software and hardware results affirm the superior response of VBHCMC over PCMC with maximum slope compensation. The VBHCMC technique combines the advantages of peak and valley current mode controls, dynamically adjusting the hysteresis band to accommodate varying load impedances. This ensures stable and precise output power regulation, significantly reducing steady-state errors compared to conventional methods. Notably, altering output voltage does not impact frequency, showcasing consistent performance. This research contributes a robust controller for fast operations, addressing challenges posed by traditional control methods during load variations.

While the proposed VBHCMC method effectively stabilizes output power across variable load conditions, it is not without limitations. Future research should focus on optimizing the adaptive hysteresis band adjustment algorithm for faster response times and exploring the integration of advanced machine learning techniques for real-time impedance estimation. Additionally, experimental validation in a wider range of surgical scenarios would further solidify the robustness of the control method.

Future work will focus on further refining the adaptive algorithm to enhance real-time performance and exploring the integration of advanced control strategies such as neural network-based adaptive controls and fuzzy logic systems to further improve stability and robustness. The VBHCMC method presents a promising solution for overcoming the challenges associated with power control in electrosurgical applications, ultimately enhancing the safety, precision, and efficacy of surgical procedures.

ACKNOWLEDGMENT

This article has been produced in part with the financial support of the European Union under the REFRESH – Research Excellence For Region Sustainability and High-tech Industries project number CZ.10.03.01/00/22_003/0000048 via the Operational Programme Just Transition, project TN02000025 National Centre for Energy II and ExPEDite project a Research and Innovation action to support the implementation of the Climate Neutral and Smart Cities Mission project. ExPEDite receives funding from the European Union's Horizon Mission Programme under grant agreement No. 101139527. The authors also extend their appreciation to Taif University, Saudi Arabia, for supporting this work through project number (TU-DSPP-2024-25).

REFERENCES

[1] M. E. Bruley, "Challenges in preventing electrical, thermal, and radiation injuries," in *Surgical Patient Care: Improving Safety, Quality and Value*, 2017, pp. 519–553, doi: 10.1007/978-3-319-44010-1_31.
[2] S. Fahad, N. Ullah, A. J. Mahdi, and N. Ullah, "A new robust closed-loop control system for electrosurgical generators," *Res. Biomed. Eng.*, vol. 36, no. 3, pp. 213–224, Sep. 2020.
[3] P. C. Benias and D. L. Carr-Locke, "Principles of electrosurgery," in *ERCP*. Amsterdam, The Netherlands: Elsevier, 2019.
[4] K. Li, L. Lu, H. Chen, G. Jiang, H. Ding, M. Yu, and Y. Xie, "Cutting performance of surgical electrodes by constructing bionic microstriped structures," *Frontiers Mech. Eng.*, vol. 18, no. 1, pp. 1–16, Mar. 2023.
[5] H. El-Kebir, J. Ran, Y. Lee, L. P. Chamorro, M. Ostoja-Starzewski, R. Berlin, G. M. A. Cornejo, E. Benedetti, P. C. Giulianotti, and J. Bentsman, "Minimally invasive live tissue high-fidelity thermophysical modeling using real-time thermography," *IEEE Trans. Biomed. Eng.*, vol. 70, no. 6, pp. 1–9, Jun. 2023.
[6] D. A. Friedrichs, R. W. Erickson, and J. Gilbert, "A new dual current-mode controller improves power regulation in electrosurgical generators," *IEEE Trans. Biomed. Circuits Syst.*, vol. 6, no. 1, pp. 39–44, Feb. 2012.

[7] A. M. Ridha, A. J. Mahdi, J. K. Abed, and S. Fahad, "PID fuzzy control applied to an electrosurgical unit for power regulation," *J. Electr. Bioimpedance*, vol. 11, no. 1, pp. 72–80, Jan. 2020.
[8] J. Karpowicz, K. Gryz, and P. Zradziński, "Evaluating current induced in limb when managing electromagnetic hazards caused by operating electrosurgical units," in *Electromagnetic Ergonomics*. Boca Raton, FL, USA: CRC Press.
[9] A. Taheri, P. Mansoori, L. F. Sandoval, S. R. Feldman, D. Pearce, and P. M. Williford, "Electrosurgery: Part II. Technology, applications, and safety of electrosurgical devices," *J. Amer. Acad. Dermatol.*, vol. 70, no. 4, pp. 607.e1–607.e12, 2014.
[10] F. C. Meeuwsen, A. C. P. Guédon, E. A. Arkenbout, M. van der Elst, J. Dankelman, and J. J. van den Dobbelsteen, "The art of electrosurgery: Trainees and experts," *Surgical Innov.*, vol. 24, no. 4, pp. 373–378, Aug. 2017.
[11] J. C. Marín-Gabriel, R. Romito, C. Guarner-Argente, J. Santiago-García, J. Rodríguez-Sánchez, and T. Toyonaga, "Use of electrosurgical units in the endoscopic resection of gastrointestinal tumors," *Gastroenterología y Hepatología*, vol. 42, no. 8, pp. 512–523, Oct. 2019.
[12] A. L. Shiver, C. Webber, T. Sliker, P. Rushford, and A. Shaw, "Bigger is not always better: Effects of electrocautery setting on tissue injury in a porcine model," *Cureus*, vol. 14, no. 7, Jul. 2022, Art. no. 26841, doi: 10.7759/cureus.26841.
[13] S. Jensen and D. Maksimovic, "Fast tracking electrosurgical generator using two-rail multiphase buck converter with GaN switches," *IEEE Trans. Power Electron.*, vol. 32, no. 1, pp. 634–641, Jan. 2017.
[14] F. M. B. Bisinotto, R. A. Dezena, L. B. Martins, M. C. Galvão, J. M. Sobrinho, and M. S. Calçado, "Burns related to electrosurgery—Report of two cases," *Revistabrasileira de Anestesiologia*, vol. 67, no. 5, pp. 527–534, Sep. 2017.
[15] C. Bao and S. K. Mazumder, "Multiresonant-frequency filter for an electrosurgery inverter," *IEEE Trans. Power Electron.*, vol. 37, no. 6, pp. 6242–6246, Jun. 2022.
[16] M. Frivaldsky, P. Spanik, J. Morgos, and M. Pridala, "Control strategy proposal for modular architecture of power supply utilizing LCCT converter," *Energies*, vol. 11, no. 12, p. 3327, Nov. 2018.
[17] R. W. Erickson and D. Maksimovic, *Fundamentals of Power Electronics*. Switzerland: Springer, 2007.
[18] M. M. Rafiq, M. Ishfaq, M. Ali, A. Ibeas, and J. Herrera, "A closed loop robust control system for electrosurgical generators," in *Control Applications for Biomedical Engineering Systems*. New York, NY, USA: Academic, 2020.
[19] H. Sabera, A. Mahdi, and M. Hu. Nawir, "Comparative analysis of integer and fractional PID for power regulation integrated in an electrosurgical generator," *Kerbala J. Eng. Sci.*, vol. 1, no. 2, pp. 233–251, 2021.
[20] H. El-Kebir, Y. Lee, R. Berlin, E. Benedetti, P. C. Giulianotti, L. P. Chamorro, and J. Bentsman, "Online hypermodel-based path planning for feedback control of tissue denaturation in electrosurgical cutting," *IFAC-PapersOnLine*, vol. 54, no. 15, pp. 448–453, 2021.
[21] S. J. Gambhire, D. R. Kishore, P. S. Londhe, and S. N. Pawar, "Review of sliding mode based control techniques for control system applications," *Int. J. Dyn. Control*, vol. 9, no. 1, pp. 363–378, Mar. 2021.
[22] Y. Ushimaru, T. Takahashi, Y. Souma, Y. Yanagimoto, H. Nagase, K. Tanaka, Y. Miyazaki, T. Makino, Y. Kurokawa, M. Yamasaki, M. Mori, Y. Doki, and K. Nakajima, "Innovation in surgery/operating room driven by Internet of Things on medical devices," *Surgical Endoscopy*, vol. 33, no. 10, pp. 3469–3477, Oct. 2019.
[23] K. J. Wikiel, F. J. Powlan, T. S. Jones, T. N. Robinson, and E. L. Jones, "Robotic stray energy with constant-voltage versus constant-power regulating electrosurgical generators," *Surgical Endoscopy*, vol. 37, no. 1, pp. 580–586, Jan. 2023.
[24] S. Shao, L. Chen, Z. Shan, F. Gao, H. Chen, D. Sha, and T. Dragicevic, "Modeling and advanced control of dual-active-bridge DC–DC converters: A review," *IEEE Trans. Power Electron.*, vol. 37, no. 2, pp. 1524–1547, Feb. 2022.
[25] G. Nayak and S. Nath, "Unified model of peak current mode controlled coupled SIDO converters," *IEEE Trans. Ind. Electron.*, vol. 69, no. 11, pp. 11156–11164, Nov. 2022.
[26] D. K. Saini, A. Reatti, and M. K. Kazimierczuk, "Average current-mode control of buck DC–DC converter with reduced control voltage ripple," in *Proc. 42nd Annu. Conf. IEEE Ind. Electron. Soc.*, Oct. 2016, pp. 3270–3275.
[27] E. Abdelhamid, L. Corradini, P. Mattavelli, G. Bonanno, and M. Agostinelli, "Sensorless stabilization technique for peak current mode controlled three-level flying-capacitor converters," *IEEE Trans. Power Electron.*, vol. 35, no. 3, pp. 3208–3220, Mar. 2020.
[28] M. M. Al Baalharith, S. A. Alsary, M. A. B. Mosa, Y. F. Almarzouq, and S. K. Basudan, "Understanding the safe application of electrosurgery: A cross sectional study of surgeons in KSA," *J. Taibah Univ. Med. Sci.*, vol. 18, no. 3, pp. 595–599, Jun. 2023.
[29] M. M. Rafiq, A. Ibeas, and N. Ullah, "Expert knowledge-based peak current mode control of electrosurgical generators for improved output power regulation," *J. Electr. Bioimpedance*, vol. 14, no. 1, pp. 32–46, Jan. 2023.
[30] H. Vardhan, B. Akin, and H. Jin, "A low-cost, high-fidelity processor-in-the loop platform: For rapid prototyping of power electronics circuits and motor drives," *IEEE Power Electron. Mag.*, vol. 3, no. 2, pp. 18–28, Jun. 2016.

MUHAMMAD MOHSIN RAFIQ received the B.S. degree in electronics engineering from COMSATS University Islamabad, in 2013, and the M.S. degree in electrical engineering from the CECOS University of IT and Emerging Sciences, Peshawar, Pakistan, in 2017, where he is currently pursuing the Ph.D. degree. Currently, he is the Director of Innovation with Aprus Technologies Pvt. Ltd., specializing in the development and design of electrosurgical generators. His research interests include various areas within power electronics, including current mode control, integer and fractional-order control, renewable energy, and power converters.

NASIM ULLAH (Member, IEEE) received the B.Sc. degree in electrical engineering from the University of Engineering and Technology, Peshawar, in 2004, and the Ph.D. degree in mechatronics engineering from Beihang University, Beijing, China, in 2013. He is currently a Professor with the Department of Electrical Engineering, Taif University, Saudi Arabia. He has completed several research projects funded by the Deanship of Scientific Research, Taif University, and the Ministry of Education, Saudi Arabia, as a Principal Investigator (PI). He has authored/co-authored more than 200 research articles in peer-review journals and contributed several book chapters. His research interests include renewable energy, microgrid, smart grids, power electronic applications in power systems, smart transformers, robotics, and flight control systems.

LUKAS PROKOP received the Ing. degree in electrical power engineering from the Faculty of Electrical Engineering and Communication, Brno University of Technology. He is currently an Associate Professor with the Faculty of Electrical Engineering and Computer Science, VSB-Technical University of Ostrava. He is also a Research Team Member of the Czech and International Research Projects. He works as the Deputy Head of the ENET Research Center. His research interests include renewable energy sources, modern technologies, and methods in electrical power engineering and electrical measurements.

STANISLAV MISAK was born in Czech Republic, in 1978. He received the Ing. and Ph.D. degrees from the Department of Electrical Engineering, VSB-Technical University of Ostrava, in 2003 and 2007, respectively. He is currently a Professor and the CEO of the ENET Research Centre and the Centre for Energy and Environmental Technologies, VSB-Technical University of Ostrava. He holds a patent for a fault detector for medium voltage power lines. His current research interests include implementation of smart grid technologies using prediction models and bio-inspired methods.